Optical Engineering 48(11), 117208 (November 2009)

Projector calibration from the camera image point of view

Xu Zhang
Limin Zhu
Shanghai Jiao Tong University
School of Mechanical Engineering
State Key Laboratory of Mechanical System and Vibration
Shanghai 200240 China
E-mail: zhulm@sjtu.edu.cn

Abstract. The traditional projector calibration always assumes that the reprojection errors on the projector image are independent and identically distributed and utilize the same method as the camera calibration. Actually, even if the measured points on the camera image are independent and identically distributed Gaussian variables, it is impossible to obtain the statistical characteristics of the reprojection errors on the projector image, because the relation between the original measurement error and the reprojection error is nonlinear. We propose a method to estimate the projector parameters according to the camera image reprojection error. It does not require us to know the statistical characteristics of the projector image point and makes full use of the background knowledge of the camera image noise, because our cost function does not concern the reprojection error on the projector image as is the case in the traditional method. The simulations and experiments affirm that this method has higher precision, even if the real noise is not normal.
 [DOI: 10.1117/1.3265551]

Subject terms: projector calibration; structured light system; bundle adjustment.

Paper 090537R received Jul. 16, 2009; revised manuscript received Sep. 30, 2009; accepted for publication Oct. 2, 2009; published online Nov. 25, 2009.

1 Introduction

The structured light method, including both projected coded light and sinusoidal fringe techniques, is the most widely used active method in the field of optical 3-D measurement. The structured light system (SLS) is always composed of a camera and a structured light projector.[1,2] In the last two decades, hundreds of systems have been developed and various products are available in the market.[3,4]

The SLS calibration is a necessary step to extract accurate metric information from 2-D images. This often includes two separate stages: camera calibration and projector calibration. Camera calibration has been extensively studied in the computer vision and photogrammetry communities.[5–8] The main difficulty of calibrating the SLS is the projector calibration. Because the projector can not "see" images like a camera and is just able to project images, determining the correspondence between the projector image and the 3-D points is more difficult. The general method to solve the problem is to use a calibrated camera to calibrate the projector. A specific pattern image is projected onto a 3-D calibration object by the projector and the pattern modulated by the 3-D calibration object is captured by the camera. Generally, it is easy to determine the correspondence between the camera image and the projector image using the pattern codification strategies[9] such as Gray code, De Bruijn, M-array, or others. Because the camera intrinsic and extrinsic parameters have been determined, the 3-D point coordinates corresponding to the camera image feature points can be computed easily. Currently, the projector can be calibrated using the observations, including both the projector image feature points and the 3-D point coordinates. This method is simple, convenient, and very practical, but the accuracy of the projector calibration is influenced by that of the camera calibration.

Projector calibration is a process of finding the true parameters of the projector model from the available observations. Three aspects, such as models, observations, and estimation methods, are indispensable.

1.1 *Model*

In the laser pot technique, the line model is usually used and six parameters (three for the center and three for the direction) are enough. In the light-stripe method, the projector model is a plane. Its parameters include the center coordinate and the plane direction. In the plane structured light technique, the projector can be regarded as the inverse of a camera, so its model is the same as the camera model. The most commonly used models are the pinhole model and the nonlinear model with lens distortion. It is clear that the line model and the plane model are just the special cases of the pinhole model.

1.2 *Observations*

Observations include the image points on the projector image and the corresponding 3-D points. To acquire the 3-D points, various calibration objects are utilized. According to the dimensions of the calibration objects, we can classify those techniques roughly into three categories:

1. *Three-dimensional reference-object-based calibration*. Calibration is performed by projecting pattern light onto a calibration object with 3-D geometry. Examples include noncoplanar lines,[10,11] a motorized mobile plane,[12] some known world planes,[13] some-

0091-3286/2009/$25.00 © 2009 SPIE

thing with a 3-D movable platform,[14] and 3-D calibration targets with known geometry.[15]

2. *Two-dimensional plane-based calibration*. Techniques in this category require a planar pattern shown at a few different orientations. At each orientation, the projector projects a known image onto the plane object and the camera observes the planar pattern. Either the SLS sensor or the planar target can be freely moved and the motion is not required to be known. Compared with the classical techniques, which use expensive 3-D reference objects, this kind of technique[16–20] is flexible and easy to implement.
3. *Self-calibration*. Techniques in this category do not require any calibration object, and can be considered a 0-D approach because only image point correspondences are required. The object is successively illuminated with grating sequences from at least two different directions, and then the geometrical constraints independent of the scene geometry are obtained.[21–23] Based on these constrains, the projector parameters and the 3-D coordinates can be calculated simultaneously. Although no calibration object is necessary, a large number of parameters must to be estimated, resulting in a much harder mathematical problem.

1.3 *Estimation Methods*

According to the estimation methods, we can classify the projector calibration approaches roughly into three kinds:

1. *Least-squares method in 3-D space*. The parameters of both the line model and the plane model can be estimated from the 3-D observations using the least-squares method.[15,16,20]
2. *Least-squares method in 2-D space of the projector image*. These techniques[18,19] employ the projector linear model and do not consider the lens distortion. The reprojection errors, the distances between the projector image points, and the modeled projections are minimized using a least-squares method. It is simple and rapid; however, the precision is limited.
3. *Bundle adjustment in 2-D space of the projector image*. Nonlinear model considering lens distortion is adoped.[17] First, the initial values of the parameters are computed using the linear model. Second, all the parameters are optimized using the bundle adjustment method[24] to minimize an objective (cost) function measuring the reprojection errors on the projector image. There are many estimation methods in the bundle adjustment. Generally, maximum likelihood (ML) estimation is used in traditional projector calibration, where the distributions of the reprojection errors on the projector image are assumed to be independent and identically distributed (i.i.d) Gaussian (normal) distributions. Thus, the ML estimation is transformed to a nonlinear least-squares problem. Since the first two kinds of estimation methods do not adopt the nonlinear model and do not consider the statistical characteristic of the measurement error, the precision of the estimated parameters is generally lower than that of the third method.

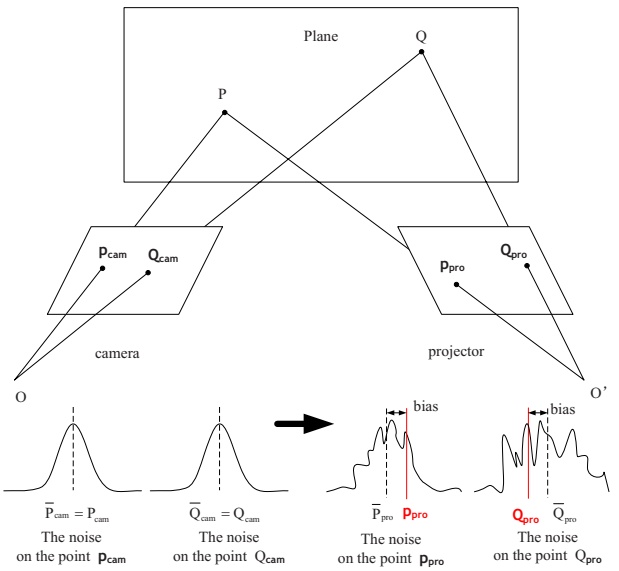

Fig. 1 Schematic diagram of the transformation from the camera image noise to the reprojection error on the projector image.

The bundle adjustment is successful for camera calibration because the camera, as a sensor, measures the feature points and the assumption about the measured points, i.i.d normal, is appropriate. However, there is a misgiving for the projector if the same method is applied. The reprojection error on the projector image is actually not i.i.d Gaussian, as required by the traditional methods, even if the points measured by the camera are i.i.d Gaussian. Figure 1 shows the SLS and the reprojection error on the projector image transformed from the noise on the camera image. The measurement points are first transformed to the 3-D space points, and then transformed to the 2-D points on the projector image. Thus, the reprojection point on the projector image is a nonlinear function of the camera measurement point, even if the camera model and projector model are the pinhole models. In this noise transformation process, the camera image noise is coupled with the camera parameters, the plane parameters, and the projector parameters. Before calibration, the projector parameters are unknown, so there is no way to determine the statistical characteristics of the reprojection error on the projector image. Generally, we can judge that the reprojection error on the projector is not normal variable and the homogeneity of the variance is also not satisfied, because the relation between the projector image point and the camera measurement point is a nonlinear function. Thus, the nonlinear least-squares method applied to calibrate the projector in the traditional method has no statistical significance. Incorrect modeling of the reprojection error on projector image is likely to disturb the ML estimate. It always leads to biased parameter estimates and lower precision results. In the other hand, the measurement points in the camera image can be assumed i.i.d normal, because the measurement noise is independent in the camera system. Thus, a problem appears naturally as to whether we can calibrate the projector from the camera image point of view. The answer is definitely yes. In this paper, we introduce a method to es-

timate the projector parameters in the space of the camera image instead of that of the projector image and prove this method is effective and has higher precision estimation through lots of simulations and real experiments.

This paper is structured as follows. Section 2 gives a simple introduction of the camera and projector model. Section 3 explains our motivation and describes our projector calibration method. Simulations and experiments are shown in the Secs. 4 and 5. The final section gives the conclusion.

2 Model Structured Light System

2.1 *Model Camera and Projector*

The model of the projector is the same as the camera model, since the projector can be conceptually regarded as a camera acting in reverse. Through the following transformations, a 3-D point $\mathbf{p}_w=[X_w,Y_w,Z_w]^T$ is mapped to the 2-D pixel $\mathbf{m}=[u,v]^T$ on the camera or projector image.

First is the transformation from the world coordinate system to the device coordinate system:

$$\tilde{\mathbf{p}}_* = \begin{bmatrix} \mathbf{R} & \mathbf{t} \\ 0 & 1 \end{bmatrix} \cdot \tilde{\mathbf{p}}_w, \tag{1}$$

where $\tilde{\mathbf{p}}_w=[X_w,Y_w,Z_w,1]^T$, and $\tilde{\mathbf{p}}_*=[X_*,Y_*,Z_*,1]^T$ denotes the homogeneous coordinates of the 3-D point in world coordinate system and the device coordinate system, respectively. For example, $\tilde{\mathbf{p}}_c$ is in the camera coordinate system, and $\tilde{\mathbf{p}}_p$ is in the projector coordinate system. Note that $\mathbf{R}$ is the rotation matrix, $\mathbf{t}$ is the translation vector, and $[\mathbf{R},\mathbf{t}]$ are called the extrinsic parameters.

Second is the normalized (pinhole) projection:

$$\begin{bmatrix} u_n \\ v_n \end{bmatrix} = \begin{bmatrix} X_*/Z_* \\ Y_*/Z_* \end{bmatrix}, \tag{2}$$

where $\mathbf{m}_n=[u_n,v_n]^T$ is the normalized image point.

Third is lens distortion. The lens distortion includes the radial distortion and tangential distortion. It is modeled as

$$\mathbf{m}_d = \mathbf{m}_n + f_n(\mathbf{m}_n,\delta),$$

$$f_n(\mathbf{m}_n,\delta) = (k_1 r^2 + k_2 r^4)\mathbf{m}_n + \begin{bmatrix} 2p_1 u_n v_n + p_2(r^2+2u_n^2) \\ p_1(r^2+2v_n^2) + 2p_2 u_n v_n \end{bmatrix},$$

$$r^2 = u_n^2 + v_n^2. \tag{3}$$

Fourth is conversion into the pixel coordinate:

$$\tilde{\mathbf{m}} = \mathbf{K}\tilde{\mathbf{m}}_d, \quad \text{where} \quad \mathbf{K} = \begin{bmatrix} \alpha & \gamma\cdot\beta & u_0 \\ 0 & \beta & v_0 \\ 0 & 0 & 1 \end{bmatrix}. \tag{4}$$

Here $\tilde{\mathbf{m}}$ and $\tilde{\mathbf{m}}_d$ are the homogeneous coordinates, $\mathbf{K}$ is the camera intrinsic matrix, $[u_0,v_0]$ are the coordinates of the principal point, α and β are the scale factors in the image u and v axes, and γ describes the skewness of the two image axes.

2.2 *Model Structured Light System*

In the structured light system, there are two processes. One is the projector emits the light onto a 3-D object. The other is the camera images the pattern modulated by the 3-D object. Here, just the method of the 2-D-plane-based calibration is discussed. The method of 3-D-reference-object-based calibration is similar. A projector image pixel $\tilde{\mathbf{m}}$ is projected onto the 2-D plane, the pose of which is unknown. The intersection point is denoted by $\mathbf{p}_w=[X_w,Y_w,Z_w]^T$ in the world coordinate system. Then, the camera captures its image $\tilde{\mathbf{m}}'$. The second process is the same as that described in the Sec. 2.1 The first process is just the reverse of the second process and seems easy. However, the steps of normalized (pinhole) projection and lens distortion do not have the reverse functions. Thus, we must explain how to determine the unique 3-D point on the plane.

2.2.1 *Transformation from the projector image to the plane*

Because $\mathbf{K}$ is nonsingular, the invertible matrix exists. Using the Eq. (4), $\tilde{\mathbf{m}}_d$ can be computed:

$$\tilde{\mathbf{m}}_d = \mathbf{K}^{-1}\tilde{\mathbf{m}}. \tag{5}$$

The analytical inversion of Eq. (3) does not exist, however, we can approximate it using the iterative method.[25,26] The iteration equations are given as

$$\tilde{\mathbf{m}}_n = \tilde{\mathbf{m}}_d - f_n(\mathbf{m}_d,\delta),$$

$$\tilde{\mathbf{m}}_d = \tilde{\mathbf{m}}_n. \tag{6}$$

Without loss of generality, the model plane is chosen as the X-Y plane of the world coordinate system, i.e., $Z_w=0$ for the points on the model plane. Denote the i'th column of the rotation matrix $\mathbf{R}$ by $\mathbf{r}_i$. From Eqs. (1) and (2), we have

$$\begin{bmatrix} u_n \\ v_n \\ 1 \end{bmatrix} = \frac{1}{Z_*}[\mathbf{r}_1 \quad \mathbf{r}_2 \quad \mathbf{r}_3 \quad \mathbf{t}] \begin{bmatrix} X_w \\ Y_w \\ 0 \\ 1 \end{bmatrix} = \frac{1}{Z_*}[\mathbf{r}_1 \quad \mathbf{r}_2 \quad \mathbf{t}] \begin{bmatrix} X_w \\ Y_w \\ 1 \end{bmatrix}. \tag{7}$$

From Eq. (7), we can get

$$\begin{bmatrix} X_w \\ Y_w \\ 1 \end{bmatrix} = \begin{bmatrix} X'/Z' \\ Y'/Z' \\ Z'/Z' \end{bmatrix},$$

$$\text{where} \quad \begin{bmatrix} X' \\ Y' \\ Z' \end{bmatrix} = [\mathbf{r}_1 \quad \mathbf{r}_2 \quad \mathbf{t}]^{-1} \begin{bmatrix} u_n \\ v_n \\ 1 \end{bmatrix}. \tag{8}$$

Generally, the matrix $\mathbf{A}=[\mathbf{r}_1,\mathbf{r}_2,\mathbf{t}]$ is nonsingular. If the matrix $\mathbf{A}$ is singular, that means the vector $\mathbf{t}$ is on the plane that is determined by vectors $\mathbf{r}_1$ and $\mathbf{r}_2$. In this situation, the 3-D plane passes though the focal center and the image of

the model plane will become a line. This degenerate case is impossible in the SLS, because the light emitted by the projector can not intersect with the model plane. Generally, Z_* does not equal 0, because it is the z coordinate of the 3-D point in the projector coordinate system. If $Z_*=0$, the 3-D point is on the projector image plane. This situation would not happen in the SLS, because the planar target is always far away from the projector and camera.

2.2.2 *Parameters of the SLS model*

The camera and projector extrinsic parameters are not all independent. They satisfy the rigid motion constraints. The relative pose between the camera and projector is denoted by $[\mathbf{R}_{pc},\mathbf{t}_{pc}]$. The projector extrinsic parameters can be represented as

$$\begin{bmatrix} \mathbf{R}_p^i & \mathbf{t}_p^i \\ 0 & 1 \end{bmatrix} = \begin{bmatrix} \mathbf{R}_{pc}\mathbf{R}_c^i & \mathbf{R}_{pc}\mathbf{t}_c^i + \mathbf{t}_{pc}^i \\ 0 & 1 \end{bmatrix}, \tag{9}$$

where $[\mathbf{R}_p^i,\mathbf{t}_p^i]$ and $[\mathbf{R}_c^i,\mathbf{t}_c^i]$ denote the camera and projector extrinsic parameters for the i'th position of the planar object, respectively. This rigid motion constraint decreases the number of parameters to be calibrated.

The parameters of the SLS model include the camera and projector intrinsic parameters, the relative pose between the camera and projector, and the camera extrinsic parameters relative to each plane pose. Among them, the camera extrinsic parameters are nuisance parameters, which are useless to obtain metric information.

3 Proposed Calibration Method

3.1 *Motivation*

Sec. 2 introduced the process of transferring from the projector image point to the camera image point in the SLS. Reprojection on the projector image from the camera measurement point is the inverse of the preceding process. It can be represented as a function $g(\,)$. The reprojection error is the difference between the model point and the actual point.

$$\mathbf{e}_p = g(\mathbf{m}',\Psi_{\text{cam}},\Psi_{\text{pro}}) - \mathbf{m}, \tag{10}$$

where Ψ_{cam} and Ψ_{pro} denote the parameters of the camera and projector, respectively; $\mathbf{m}$ is the model point on the projector image; and $\mathbf{m}'$ is the camera measurement point. We can see the reprojection error on the projector image is a nonlinear function of the measurement point on the camera image. We assume that the observations are the random variables, which are the summation of the theory values and i.i.d normal noise. Taking derivation of the function in Eq. (10), we have

$$\Delta\mathbf{e}_p = \Delta g(\overline{\mathbf{m}'},\Psi_{\text{cam}},\Psi_{\text{pro}})\cdot\Delta\overline{\mathbf{m}'}, \tag{11}$$

where $\overline{\mathbf{m}'}$ denotes the expectation of the measurement points, and $\Delta g(\,)$ is the derivative function of $g(\,)$. The covariance matrix of reprojection error on projector image is

$$\begin{aligned}\mathbf{W}_{ij} &= \Delta g(\overline{\mathbf{m}'_{ij}},\Psi_{\text{cam}},\Psi_{\text{pro}})\cdot\Delta\overline{\mathbf{m}'}_{ij}\cdot\Delta\overline{\mathbf{m}'}_{ij}^{T}\cdot\Delta g(\overline{\mathbf{m}'}_{ij},\Psi_{\text{cam}},\Psi_{\text{pro}})^T \\ &= \lambda\Delta g(\overline{\mathbf{m}'_{ij}},\Psi_{\text{cam}},\Psi_{\text{pro}})\cdot\Delta g(\overline{\mathbf{m}'}_{ij},\Psi_{\text{cam}},\Psi_{\text{pro}})^T,\end{aligned} \tag{12}$$

where λ is a scalar and the same for every measurement point. The index i denotes the i'th frame image, and the index j denotes the j'th measured point. Because the $\Delta g(\,)$ is the function of $\overline{\mathbf{m}}'_{ij}$, the variances of the different reprojection points are different, depending on the expectation of the measured point. So the cost function of ML estimation on the projector image should be the sum of the squared covariance-weighted prediction errors:

$$f(\Psi_{\text{pro}}) = \frac{1}{2}\sum_{i,j}\mathbf{e}_p^T\mathbf{W}_{ij}\mathbf{e}_p. \tag{13}$$

For calibrating the projector, we require the covariance matrix of each point, while for calculating the covariance matrix, the projector parameters Ψ_{pro} should be availble. This contradiction is bothersome to find a practical pipeline for projector calibration. Now, most projector calibration methods assume all the $\mathbf{W}_{ij}$ matrices are identity matrices, resulting in a simplified version of the cost function of Eq. (13), and the same method as the camera calibration is used. These methods are easy implement and can compute the projector parameters. However, incorrect modeling of the reprojection error on the projector image is likely to disturb the ML estimate. This always leads to biased parameter estimates and lower precision results. To deal with this problem, we propose a method to estimate the projector parameters according to the reprojection error in the space of the camera image instead of that in the space of the projector image.

3.2 *Framework*

Our algorithm for SLS calibration also has two parts: camera calibration and projector calibration. The framework is described as follows.

1. Camera calibration using Zhang's method.[8]
2. The corresponding 3-D points on the plane are computed from the feature points on the camera image. Since the camera parameters have been determined in the step 1, the point transformation from the camera image to the plane is easily performed by the Eqs. (5)–(8).
3. The initial values of the projector parameters are acquired using the linear method.[8]
4. Bundle adjustment on the camera image.
5. SLS calibration using bundle adjustment on the camera image for augmented data.

3.3 *Getting the Initial Values of the Projector Parameters*

Without considering the lens distortion, from the Eqs. (1), (2), and (4), the projector can be modeled as

$$\lambda\tilde{\mathbf{m}} = \mathbf{K}[\mathbf{R},\mathbf{t}]\tilde{\mathbf{p}}_w, \tag{14}$$

where λ is an unknown scalar. The homography between the projector image and the 3-D plane pattern can be represented as

$$\mathbf{H} = \mathbf{K}[\mathbf{r}_1, \mathbf{r}_2, \mathbf{t}]. \tag{15}$$

Let's denote the homography by $\mathbf{H}=[\mathbf{h}_1, \mathbf{h}_2, \mathbf{h}_2]$. Using the knowledge that $\mathbf{r}_1$ and $\mathbf{r}_2$ are orthonormal, we have

$$\mathbf{h}_1^T(\mathbf{K}^{-1})^T\mathbf{K}^{-1}\mathbf{h}_2 = 0, \tag{16}$$

$$\mathbf{h}_1^T(\mathbf{K}^{-1})^T\mathbf{K}^{-1}\mathbf{h}_1 = \mathbf{h}_2^T(\mathbf{K}^{-1})^T\mathbf{K}^{-1}\mathbf{h}_2. \tag{17}$$

There are the two basis constraints on the intrinsic parameters, given one homography. The number of the intrinsic parameters is 5, so at least three pieces of homography are required. Using a linear least-squares method such as the singular value decomposition, the matrix $(\mathbf{K}^{-1})^T\mathbf{K}^{-1}$ can be computed, then using Cholesky factorization or a direct algebra method such as Zhang's,[8] the projector intrinsic parameters $\mathbf{K}$ can be calculated. Once $\mathbf{K}$ is known, the extrinsic parameters for each image are readily computed. From Eq. (15), we have

$$\mathbf{r}_1 = \lambda\mathbf{K}^{-1}\mathbf{h}_1,$$

$$\mathbf{r}_2 = \lambda\mathbf{K}^{-1}\mathbf{h}_2,$$

$$\mathbf{r}_3 = \mathbf{r}_1 \times \mathbf{r}_2,$$

$$\mathbf{t} = \lambda\mathbf{K}^{-1}\mathbf{h}_3, \tag{18}$$

where

$$\lambda = 1/\|\mathbf{K}^{-1}\mathbf{h}_1\| = 1/\|\mathbf{K}^{-1}\mathbf{h}_2\|.$$

Of course, because of noise in data, the so-computed matrix $\mathbf{R}=[\mathbf{r}_1, \mathbf{r}_2, \mathbf{r}_3]$ does not in general satisfy the properties of a rotation matrix. The best rotation matrix approximating a general 3×3 matrix can be estimated using the singular value decomposition. A detailed explanation can be found in Ref. 8 Knowing the camera and projector extrinsic parameters, we can compute the relative pose from the camera to the projector from Eq. (9). Now an initial guess of $\mathbf{K}$ and $[\mathbf{R}_{pc}, \mathbf{t}_{pc}]$ can be obtained using the linear method.

Actually, a common projector always has lens distortion, especially at the periphery. An initial value of the lens distortion can be simply set $\mathbf{0}$, i.e., $[k_1, k_2, p_1, p_2]=\mathbf{0}$. These are optimized in the next subsection concerning bundle adjustment on the camera image. In our experiments, we find these initial values are enough good for an off-the-shelf projector.

3.4 *Bundle Adjustment on the Camera Image*

The camera image reprojection error can be formulized as

$$\mathbf{e}_c = \mathbf{m}' - g^{-1}(\mathbf{m}, \Psi_{\text{cam}}, \Psi_{\text{pro}}), \tag{19}$$

where $g^{-1}(\,)$ denotes the transformation from the projector image to the camera image; Ψ_{cam} and Ψ_{pro} denote the parameters of the camera and projector, respectively; $\mathbf{m}$ is the model point on the projector image; $\mathbf{m}'$ is the camera measurement point; $\mathbf{m}$ is deterministic and known before; and Ψ_{cam} is computed in the process of camera calibration. Our cost function for projector calibration is

$$f(\Psi_{\text{pro}}) = \frac{1}{2}\sum_{i,j}\mathbf{e}_c^T\mathbf{e}_c. \tag{20}$$

Minimizing Eq. (20) is a nonlinear minimization problem, which can be solved by the Levenberg-Marquardt method.[27] Our method does not require us to compute the covariance matrices of the reprojection error on the projector image and makes full use of the background knowledge of measurement points.

3.5 *SLS Calibration Using Bundle Adjustment on the Camera Image for Augmented Data*

With our method, the cost functions for camera and projector calibrations are both about the reprojection errors on the camera image. They have the same formula. Because more data will increase the precision of the ML estimation, the augmented data including the 3-D points for camera calibration and 2-D points for projector calibration is incorporated to optimize the SLS parameters. The cost function is

$$f(\Psi_{\text{cam}}, \Psi_{\text{pro}}) = \frac{1}{2}\sum_{i,j}\mathbf{e}_c'^T\mathbf{e}_c' + \frac{1}{2}\sum_{i,j}\mathbf{e}_c^T\mathbf{e}_c, \tag{21}$$

where $\mathbf{e}_c'=\mathbf{m}'-q(\mathbf{p}_w, \Psi_{\text{cam}})$, and $q(\,)$ denotes the transformation from 3-D point on the calibration plane, i.e., $\mathbf{p}_w$, to the camera image.

3.6 *Remarks about the Model of the Lens Distortion for the Projector*

The transformation from the distorted image point to the normalized image point is complex, described in the Sec. 2. The iterative method is time-consuming and will lead to many high-order terms. For example, the degree of the polynomial increases from 4 to 16 after one piece of iteration. This will result in instability of the solution when the cost functions of Eqs. (20) and (21) are employed. Thus, another model of the lens distortion[25,28] for the projector is used:

$$\tilde{\mathbf{m}}_n = \tilde{\mathbf{m}}_d + f_d(\mathbf{m}_d, \delta),$$

$$f_d(\mathbf{m}_d, \delta) = (k_1 r_d^2 + k_2 r_d^4)\mathbf{m}_d + \begin{bmatrix} 2p_1u_dv_d + p_2(r_d^2 + 2u_d^2) \\ p_1(r_d^2 + 2v_d^2) + 2p_2u_dv_d \end{bmatrix},$$

$$r_d^2 = u_d^2 + v_d^2, \tag{22}$$

where $\mathbf{m}_d$ is the distorted image point, and $\mathbf{m}_n$ is the normalized image point. The parameters k_1 and k_2 are the coefficients for the radial distortion that causes the actual image point to be displaced radially on the image plane, and the parameters p_1 and p_2 are the coefficients for the decentering or tangential distortion that may occur when the centers of the curvature of the lens surface in the lens system are not strictly collinear.

In computation of $g^{-1}(\,)$, Eqs. (22) are used instead of the iterative method, Eqs. (6).

3.7 *Precision Evaluation Method*

The standard deviations of the estimated parameters should be given in practical application. Our previous work[29] described a theoretical framework for evaluating the precision for camera calibration. Now we apply this method to analyze the uncertainty of the proposed projector calibration algorithm. The covariance matrix of the projector parameters can be denoted as

$$\sum_{\Delta\Psi_{\text{pro}}} = \mathbf{J}^{-1}\Delta\mathbf{X}\cdot\Delta\mathbf{X}^T(\mathbf{J}^{-1})^T,$$

where

$$\mathbf{J} = \begin{bmatrix} \dfrac{\partial g_1^{-1}(\mathbf{m},\Psi_{\text{cam}},\Psi_{\text{pro}})}{\partial\Psi_{\text{pro}}} \\ \vdots \\ \dfrac{\partial g_n^{-1}(\mathbf{m},\Psi_{\text{cam}},\Psi_{\text{pro}})}{\partial\Psi_{\text{pro}}} \end{bmatrix}, \quad \Delta\mathbf{X} = \begin{bmatrix} \Delta\mathbf{m}_1' \\ \vdots \\ \Delta\mathbf{m}_n' \end{bmatrix}. \tag{23}$$

For the augmented data, the covariance matrix of the SLS parameters can be expressed as

$$\sum_{\Delta\Psi_{\text{pro}},\Psi_{\text{cam}}} = \mathbf{J}_{au}^{-1}\Delta\mathbf{X}_{au}\cdot\Delta\mathbf{X}_{au}^T(\mathbf{J}_{au}^{-1})^T,$$

where

$$\mathbf{J}_{au} = \begin{bmatrix} \dfrac{\partial g_1^{-1}(\mathbf{m},\Psi_{\text{cam}},\Psi_{\text{pro}})}{\partial\Psi_{\text{pro}}} & \dfrac{\partial g_1^{-1}(\mathbf{m},\Psi_{\text{cam}},\Psi_{\text{pro}})}{\partial\Psi_{\text{cam}}} \\ \vdots & \vdots \\ \dfrac{\partial g_n^{-1}(\mathbf{m},\Psi_{\text{cam}},\Psi_{\text{pro}})}{\partial\Psi_{\text{pro}}} & \dfrac{\partial g_n^{-1}(\mathbf{m},\Psi_{\text{cam}},\Psi_{\text{pro}})}{\partial\Psi_{\text{cam}}} \\ 0 & \dfrac{\partial q_1(\mathbf{p}_w,\Psi_{\text{cam}})}{\partial\Psi_{\text{cam}}} \\ \vdots & \vdots \\ 0 & \dfrac{\partial q_{n'}(\mathbf{p}_w,\Psi_{\text{cam}})}{\partial\Psi_{\text{cam}}} \end{bmatrix},$$

$$\Delta\mathbf{X}_{au} = \begin{bmatrix} \Delta\mathbf{m}_1' \\ \vdots \\ \Delta\mathbf{m}_n' \\ \Delta\mathbf{m}_1' \\ \vdots \\ \Delta\mathbf{m}_{n'}' \end{bmatrix}. \tag{24}$$

For the convenience of comparing two projector calibration methods, the method the precision evaluation for the traditional projector calibration is also presented. Its covariance matrix can be denoted as

$$\sum_{\Delta\Psi_{\text{pro}}} = \mathbf{J}_{\text{tra}}^{-1}\Delta\mathbf{X}_{\text{tra}}\cdot\Delta\mathbf{X}_{\text{tra}}^T(\mathbf{J}_{\text{tra}}^{-1})^T,$$

where

$$\mathbf{J}_{\text{tra}} = \begin{bmatrix} \dfrac{\partial g_1(\mathbf{m}',\Psi_{\text{cam}},\Psi_{\text{pro}})}{\partial\Psi_{\text{pro}}} \\ \vdots \\ \dfrac{\partial g_n(\mathbf{m}',\Psi_{\text{cam}},\Psi_{\text{pro}})}{\partial\Psi_{\text{pro}}} \end{bmatrix}, \quad \Delta\mathbf{X}_{\text{tra}} = \begin{bmatrix} \Delta\mathbf{m}_1 \\ \vdots \\ \Delta\mathbf{m}_n \end{bmatrix} \tag{25}$$

Similarly, the covariance matrix of the camera parameters using Zhang's method[8] can be denoted as

$$\sum_{\Delta\Psi_{\text{cam}}} = \mathbf{J}_{\text{cam}}^{-1}\Delta\mathbf{X}_{\text{cam}}\cdot\Delta\mathbf{X}_{\text{cam}}^T(\mathbf{J}_{\text{cam}}^{-1})^T,$$

where

$$\mathbf{J}_{\text{cam}} = \begin{bmatrix} \dfrac{\partial q_1(\mathbf{p}_w,\Psi_{\text{cam}})}{\partial\Psi_{\text{cam}}} \\ \vdots \\ \dfrac{\partial q_{n'}(\mathbf{p}_w,\Psi_{\text{cam}})}{\partial\Psi_{\text{cam}}} \end{bmatrix}, \quad \Delta\mathbf{X}_{\text{cam}} = \begin{bmatrix} \Delta\mathbf{m}_1' \\ \vdots \\ \Delta\mathbf{m}_{n'}' \end{bmatrix}. \tag{26}$$

4 Simulations

The simulated camera has the following properties: $\alpha=1100$, $\beta=1100$, $\gamma=0$, $u_0=500$, and $v_0=500$. The image resolution is 1000×1000. The simulated projector has the following properties: $\alpha=1200$, $\beta=1200$, $\gamma=0$, $u_0=512$, and $v_0=800$. The image resolution is 1024×768. We can see that the whole projector image is above the principal point, because the off-the-shelf projectors always have this setup to make the projection image on a higher position than the projector. The model plane has two parts. The left is a chessboard pattern containing $14\times28=392$ corner points. The size of square is 50×50 mm. The right is blank as the projecting screen. Only the projected pattern in this area is valid and others outside this area will be deleted.

The orientation of the plane is represented by a 3-D vector **om**, which is parallel to the rotation axis and whose magnitude is equal to the rotation angle. Its position is represented by a 3-D vector **t** (unit in millimeters). In this experiment, we use three planes with $\mathbf{om}_1=[0.3491,0,0]^T$, $\mathbf{om}_2=[0,0.3491,0]^T$, $\mathbf{om}_3=[-0.2618,-0.2618,-0.1309]^T$, $\mathbf{t}_1=[-700,-700,1500]^T$, $\mathbf{t}_2=[-700,-700,1510]^T$, $\mathbf{t}_3=[-700,-700,1525]^T$. The extrinsic parameters of the projector relative to the camera are $[\mathbf{om}_{pc}^T,\mathbf{t}_{pc}^T]=[0,0.2,0,-300,0,-3]$.

Some specific points are generated on the projector image. The 3-D points corresponding to them are acquired using the projector model and the corresponding 2-D points on the camera image are computed through the camera model. The 3-D corner points on the left part of the model plane are captured by the camera and the corresponding image point are also acquired using the camera model. Gaussian noise with 0 mean and σ standard deviation is added to all the projected image points on the camera image.

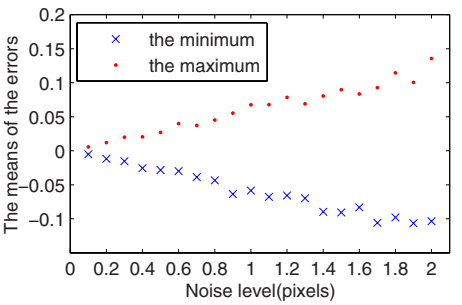

Fig. 2 Means of the reprojection errors versus noise level.

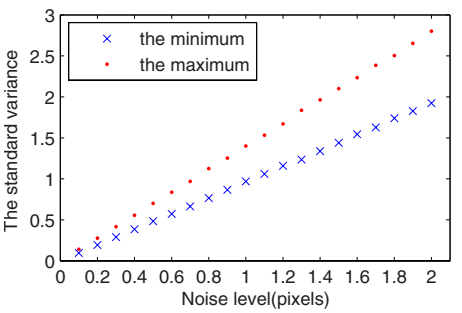

Fig. 3 Standard variance of the reprojection errors versus noise level.

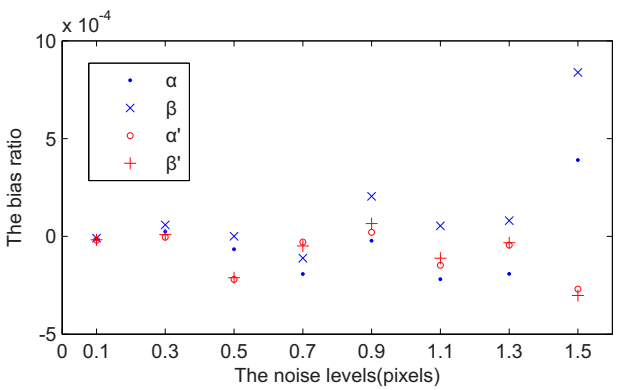

Fig. 4 Bias ratio of the scale factors versus noise level. The point and cross markers are the results from the traditional method and the circle and plus sign markers are the results from our proposed method.

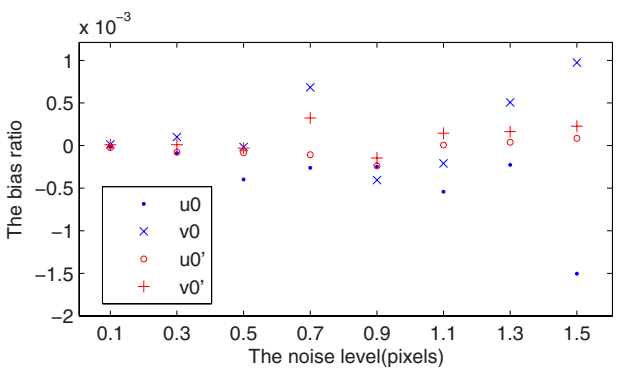

Fig. 5 Bias ratio of the principle point versus noise level. The point and cross markers are the results from the traditional method and the circle and plus sign markers are the results from our propsed method.

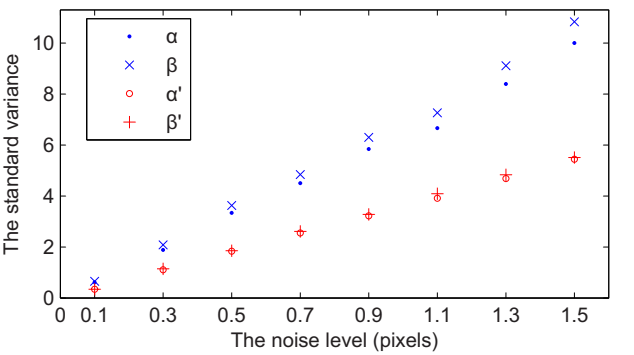

Fig. 6 Standard variance of the scale factors versus noise level. The point and cross markers are the results from the traditional method and the circle and plus sign markers are the results from our proposed method.

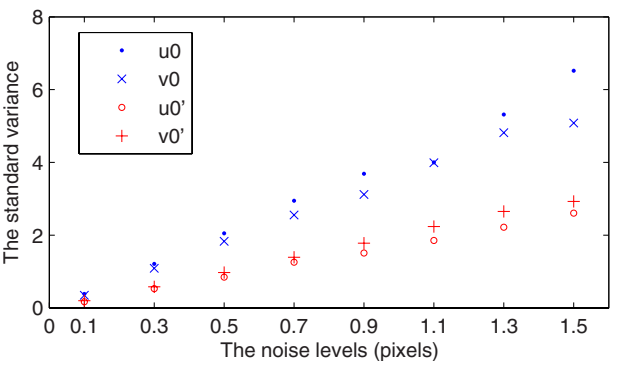

Fig. 7 Standard variance of principle point versus noise level. The point and cross markers are the results from the traditional method and the circle and plus sign markers are the results from our proposed method

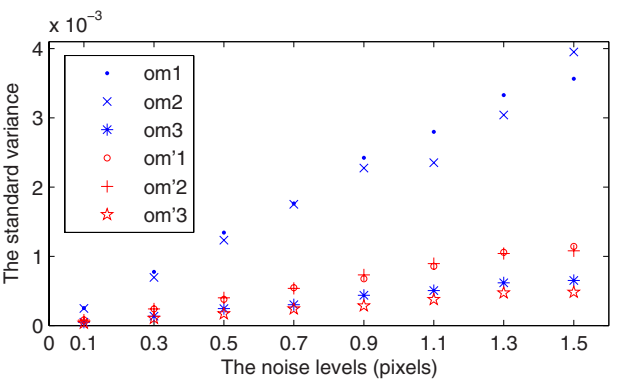

Fig. 8 Standard variance of the rotation parameters between the projector and the camera versus noise level. The point, cross and asterisk markers are the results from the traditional method and the circle, plus sign and five-point star markers are the results from our proposed method

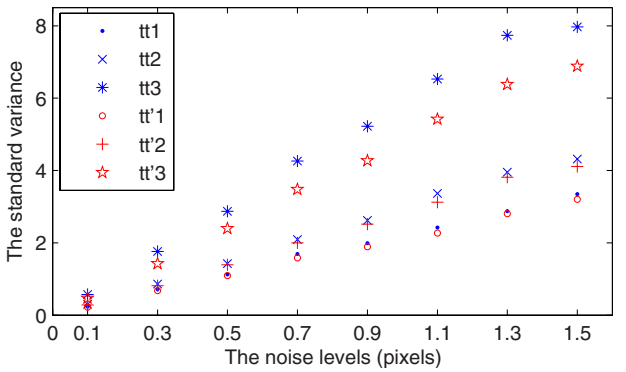

Fig. 9 Standard variance of the position parameters between the projector and the camera versus noise level. The point, cross and asterisk markers are the results from the traditional method and the circle, plus sign and five-point star markers are the results from our proposed method

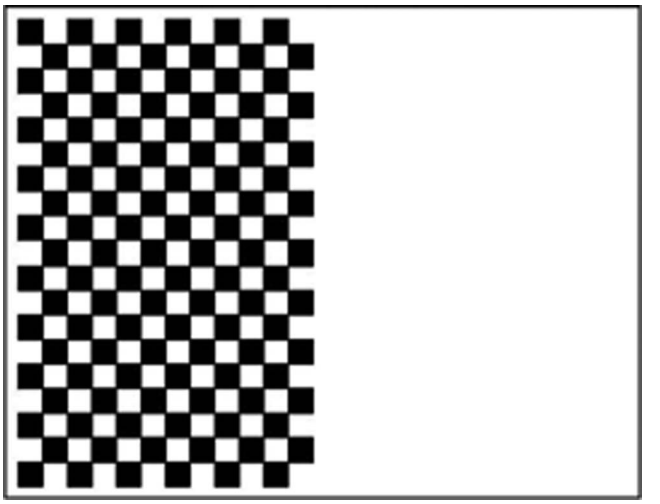

Fig. 11 Planar target.

4.1 *Statistical Characteristic of the Reprojection Error on the Projector Image*

If no noise is on the camera image, the reprojection error is also definitely 0. When i.i.d noise is added on the camera image point, the reprojection error on the projector image is a random variable, as it is transformed from the camera image noise. This experiment investigates its statistical characteristic. Five thousand times are implemented and the bias and the variance for each point are calculated. We compute the maximum and the minimum in all reprojection errors for each noise level. From the Figs. 2 and 3, we can see that the gap between the maximum and minimum becomes larger with an increase of the noise level. The bias is not exactly 0 and changes along with the point position. The variances for different points are not identical for a given noise level. In summary, the reprojection errors on different points are also different. Thus, we can not assume the reprojection error on the projector image is identical. Moreover, the reprojection errors on the projector are not normal variables, since the transformation function is nonlinear.

4.2 *Performance of Two Different Methods*

The projector calibration is performed using two methods. One is the traditional method with the optimization on the projector image. It always utilizes the same method as the

Fig. 10 Portable SLS.

0 1 2 1 1 0 1 2 2 1 2 2 2 0 0 0 1 1 0 1 1 2 2 0 0
0 1 2 1 2 2 1 0 0 2 2 2 1 0 0 0 2 2 1 1 1 2 2 2 2
2 2 0 1 2 2 1 2 1 1 0 0 0 2 2 0 0 2 2 0 2 2 1 0 0
0 0 0 0 1 2 0 1 1 1 0 0 2 0 0 0 1 1 1 0 0 0 0 2 2
2 1 1 0 0 0 0 2 1 2 1 1 2 2 2 0 1 0 1 2 1 0 2 1 1
1 1 0 2 2 0 2 2 0 0 0 0 2 1 1 0 1 2 2 0 1 1 2 2 2
2 1 1 0 2 1 0 1 0 1 1 1 0 2 2 0 0 2 0 2 1 0 2 2 2
2 0 2 2 2 0 2 0 2 1 2 2 0 2 2 0 0 2 1 1 0 1 0 1 1
1 0 1 1 0 1 1 2 0 1 1 1 1 1 1 0 2 0 1 2 0 2 0 0 0
0 2 1 2 0 2 2 2 2 0 1 1 0 0 0 0 0 0 1 2 2 1 1 2 2
2 0 2 2 1 1 2 2 1 0 2 2 1 2 2 0 2 1 0 1 0 1 0 2 2
2 2 0 1 0 1 1 0 2 2 0 0 2 2 2 0 1 0 0 0 2 2 1 2 2
2 1 1 0 1 2 0 0 2 0 1 1 1 2 2 0 2 1 2 2 1 0 2 0 0
0 2 1 2 2 0 2 1 1 2 1 1 1 0 0 0 2 2 0 2 2 1 1 0 0
0 2 1 2 1 1 2 0 0 1 1 1 2 0 0 0 1 1 2 2 2 1 1 1 1
1 1 0 2 1 1 2 1 2 2 0 0 0 1 1 0 0 1 1 0 1 1 2 0 0
0 0 0 0 2 1 0 2 2 2 0 0 1 0 0 0 2 2 2 0 0 0 0 1 1
1 2 2 0 0 0 0 1 2 1 2 2 1 1 1 0 2 0 2 1 2 0 1 2 2
2 2 0 1 1 0 1 1 0 0 0 0 1 2 2 0 2 1 1 0 2 2 1 1 1

(a)

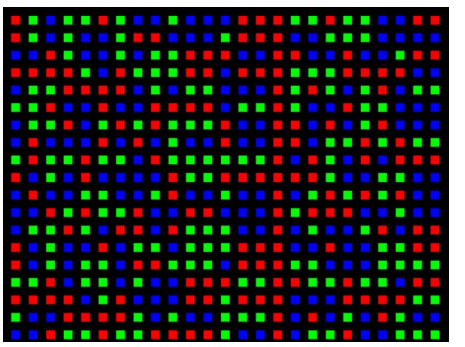

(b)

Fig. 12 M-array pattern: (a) the 19×25 code matrix and (b) the corresponding code image.

Table 1 The results of the projector calibration on three images.

	Traditional Method		Our Method	
	Value	σ	Value	σ
α	1951.8	35.5	1991.9	15.6
β	1952.4	34.7	1991.8	16.9
γ	−0.0006	0.0026	0.0012	0.0027
u_0	529.4	18.7	552.3	13.8
v_0	825.4	20.8	835.7	22.2
	0.1031	0.0087	0.1078	0.0060
$\mathbf{om}_{pc}$	−0.1315	0.0041	−0.1326	0.0034
	−0.0080	0.0009	−0.0056	0.0018
	146.83	11.27	148.36	1.47
$\mathbf{t}_{pc}$	−121.42	11.72	−118.67	1.41
	−10.48	19.87	−13.71	3.53
rms	(0.5597, 0.5628)		(0.6418, 0.6080)	

Table 3 The results of the projector calibration on five images.

	Traditional Method		Our Method	
	Value	σ	Value	σ
α	1965.3	10.4	1961.8	8.0
β	1967.3	10.6	1962.1	9.3
γ	−0.0001	0.0014	0.0012	0.0019
u_0	542.5	7.4	548.1	9.8
v_0	825.4	14.9	841.0	17.5
	0.1015	0.0071	0.1099	0.0050
$\mathbf{om}_{pc}$	−0.1319	0.0039	−0.1311	0.0027
	−0.0075	0.0008	−0.0073	0.0013
	148.70	4.32	150.16	0.54
$\mathbf{t}_{pc}$	−118.91	8.31	−118.77	0.73
	−13.97	6.23	−14.85	2.71
rms	(0.5928, 0.5771)		(0.6788, 0.6341)	

camera calibration method.[8] The other is our proposed method using the cost function evaluated on the camera image. Three hundred times are implemented and the bias ratio and the standard variance for each parameters are shown in the Figs. 4–9. From Figs. 4 and 5, we can see the biases of the parameters from two methods are both very small. They are both correct estimators. The standard variances of the projector intrinsic parameters are shown in Figs. 6 and 7. The standard variances of the estimates obtained with our method are just 55% of those obtained with the traditional method. As for the extrinsic parameters, the precision from our method is also higher than that from the traditional method, as shown in the Figs. 8 and 9.

Table 2 The results of the projector calibration on four images.

	Traditional Method		Our Method	
	Value	σ	Value	σ
α	1975.2	24.9	1968.9	12.0
β	1976.4	24.0	1970.6	13.6
γ	0.0001	0.002	0.0014	0.0023
u_0	554.2	15.2	557.1	11.4
v_0	850.5	19.8	868.3	19.3
	0.1068	−0.0089	0.1094	0.0054
$\mathbf{om}_{pc}$	−0.1359	0.0041	−0.1305	0.0030
	−0.0089	0.0008	−0.0088	0.0015
	145.30	9.08	151.36	1.04
$\mathbf{t}_{pc}$	−122.71	11.17	−120.45	1.19
	1.14	13.80	−19.86	3.33
rms	(0.5786, 0.5753)		(0.6747, 0.6271)	

5 Experiments

To compare the performance of our proposed method with the traditional method, the methods are implemented on the same SLS, as shown in Fig. 10. The SLS is composed with a camera with a 1024×1024 resolution and a digital light procession (DLP) projector with a 1024×768 resolution.

To calibrate the SLS, the model plane shown in Fig. 11 is used. For each pose of the model plane, two images, called a couple of images, are captured in two different situations. One is the gray image with an intensity of 128 is projected onto the model plane by the projector. The black and white chessboard is imaged by the camera. The other is the M-array pattern[30] is projected onto the model plane by the projector. The 26×757 pseudoarray with the 3×3 window is constructed by folding a pseudorandom sequence generated by the primitive polynomial $x^9+x^7+x^5+1$ from Galois field with 3 elements, GF(3). The M-array code and the corresponding image are shown in Fig. 12. Here, just the 19×25 submatrix is used. The pattern modulated by the model plane is imaged by the camera. To calibrate the camera and the projector, the corners of the two images are detected using the subpixel corner detection method.[31] The two projector calibration methods use the same data and the initial values of the parameters are also acquired with the

Table 4 The results of the projector calibration on six images.

	Traditional Method		Our Method	
	Value	σ	Value	σ
α	1965.3	10.2	1959.8	7.3
β	1968.0	10.3	1961.9	8.9
γ	−0.0001	0.0017	0.0017	0.0018
u_0	546.4	7.2	551.7	9.2
v_0	827.2	14.7	847.1	16.7
	0.1001	0.0070	0.1098	0.0048
$\mathbf{om}_{pc}$	−0.1328	0.0039	−0.1313	0.0027
	−0.0077	0.0008	−0.0076	0.0013
	148.81	4.22	150.39	0.50
$\mathbf{t}_{pc}$	−119.06	8.20	−118.84	0.67
	−13.33	6.09	−15.55	2.49
rms	(0.6099, 0.5887)		(0.7011, 0.6436)	

Table 5 The results of the camera calibration on three images.

	Traditional Method		Our Method	
	Value	σ	Value	σ
α	2161.6	27.6	2216.5	17.9
β	2177.3	26.6	2227.4	18.1
γ	0.0028	0.0006	0.0012	0.0007
u_0	503.4	10.3	522.2	12.4
v_0	495.1	12.9	495.7	18.4
k_1	−0.1147	0.0279	−0.0482	0.0255
k_2	0.5068	0.3255	−0.1448	0.2345
p_1	−0.0001	0.0017	−0.0009	0.0025
p_2	−0.0042	0.0018	−0.0014	0.0024
rms	(0.4182, 0.1782)		(0.5891, 0.5221)	

same method. Just the cost functions are different. The precisions of the SLS parameters with traditional method are computed using Eqs. (25) and (26), while those with our method are obtained using Eq. (24). The root of mean squared (rms) distances, in pixels, between detected and projected image points are also calculated.

Six couples of images are captured. The first 3, 4, 5, and all 6 couples of images are used to calibrate the camera and projector. The results of the projector calibration with the two methods are compared in Tables 1–4, respectively. For each method in each configuration, the estimated parameters and the estimated standard deviation are presented. The corresponding parameters in the first and third columns are nearly the same, however, the standard variances in the second column are larger than those in the fourth column. Tables 5–8 give the results for the camera calibration. The standard variances in fourth column is also smaller. From these tables, we can see the final estimate values from two method are consistent with each other whether we use 3, 4, 5, or 6 images. However, the uncertainty of the final estimate with our method is smaller than that with the traditional method whether we use 3, 4, 5, or 6 images. Especially, the standard variances of α and β reduce rapidly.

To further investigate the precision of two estimate methods, we applied them to all combinations of four couples of images from the first five couples of images. The calibrated results are applied to compute the 3-D points from the patten image in the sixth couple. In this experiment, the same corresponding points and the same planar target are utilized; just the estimated parameters from the two methods are different. Of course, because of noise in data, the so-computed parameters do not, in general, equal the real values and the so-computed 3-D points do not in general, exist on a plane. The flatness of the 3-D points can reflect the uncertainty of the SLS parameters. The results are shown in Table 9, where the standard variance and the minimum and the maximum deviation are all given for each configuration. We can see they are all very small, however, ours is even smaller. The ratios of the standard variance and the error band are less than 66.5 and 84.4%, respectively, shown in the last two rows. In summary, the flatness of the 3-D points with our method is smaller than one with traditional method.

Table 6 The results of the camera calibration on four images.

	Traditional Method		Our Method	
	Value	σ	Value	σ
α	2167.7	18.7	2202.1	13.5
β	2182.1	18.3	2217.3	13.6
γ	0.0033	0.0006	0.0025	0.0007
u_0	517.1	9.7	538.7	10.5
v_0	512.0	12.4	526.7	15.8
k_1	−0.1094	0.0222	−0.0701	0.0203
k_2	0.5341	0.2624	0.0077	0.1786
p_1	0.0026	0.0016	0.0035	0.0021
p_2	−0.0015	0.0015	−0.0004	0.0018
rms	(0.4502, 0.2637)		(0.6171, 0.5423)	

Table 7 The results of the camera calibration on five images.

	Traditional Method		Our Method	
	Value	σ	Value	σ
α	2184.5	14.2	2182.8	7.5
β	2199.2	13.4	2196.8	7.1
γ	0.0031	0.0006	0.0022	0.0005
u_0	517.8	8.4	529.3	9.2
v_0	501.3	12.4	500.4	14.5
k_1	−0.1222	0.0218	−0.0771	0.0178
k_2	0.6365	0.2779	0.0317	0.1815
p_1	0.0008	0.0016	0.0006	0.0018
p_2	−0.0031	0.0014	−0.0013	0.0016
rms	(0.5101, 0.2683)		(0.6348, 0.5472)	

Table 8 The results of the camera calibration on six images.

	Traditional Method		Our Method	
	Value	σ	Value	σ
α	2183.1	12.6	2182.2	7.1
β	2197.9	12.1	2196.3	6.8
γ	0.0033	0.0006	0.0025	0.0005
u_0	520.5	7.9	531.9	8.7
v_0	506.0	11.4	507.2	13.6
k_1	−0.1261	0.0197	−0.0798	0.0162
k_2	0.6963	0.2503	0.1057	0.1643
p_1	0.0014	0.0015	0.0016	0.0017
p_2	−0.0026	0.0012	−0.0007	0.0014
rms	(0.4838, 0.2871)		(0.6421, 0.5549)	

5.1 *Statistical Characteristic the Camera Image Noise*

In preceding section, we assume that the measurement noise is i.i.d Gaussian. In this experiment, the statistical characteristics of measurement noise are investigated. In one process of the SLS calibration, 100 couples of images are captured for just one pose of the planar target. The same methods are applied to them to obtain corners. Through the normality test, we found that the coordinates of the corners are not Gaussian. Figure 13 shows the histogram of the frequency counts for one corner point. The standard variance for each point is also computed, and these are shown in Fig. 14. We can see that the variances for the x and y coordinates are different. Although these data shows that the noise is not identical and not Gaussian, the preceding experiments showed that the estimate on the camera image is much better than that on the projector image. We believe there are two reasons for this results. First, the coupling effect between the measurement noise with the SLS system parameters are avoided. The camera is the source of real

Table 9 The flatness of image 6 from two calibrated parameters (μm).

	Traditional Method				
	(1 2 3 4)	(1 2 3 5)	(1 2 4 5)	(1 3 4 5)	(2 3 4 5)
σ	1.134	1.153	1.050	1.074	1.333
max	4.008	4.258	3.987	3.782	4.288
min	−3.692	−3.782	−3.699	−3.692	−3.710
	Our Method				
	(1 2 3 4)	(1 2 3 5)	(1 2 4 5)	(1 3 4 5)	(2 3 4 5)
σ	0.754	0.650	0.648	0.671	0.754
max	3.846	3.504	3.611	3.529	3.796
min	−2.625	−2.582	−2.590	−2.779	−2.461
	Our Method/Traditional Method (%)				
σ	66.5	56.4	61.7	62.5	56.6
error band	84.4	75.7	80.7	84.4	77.7

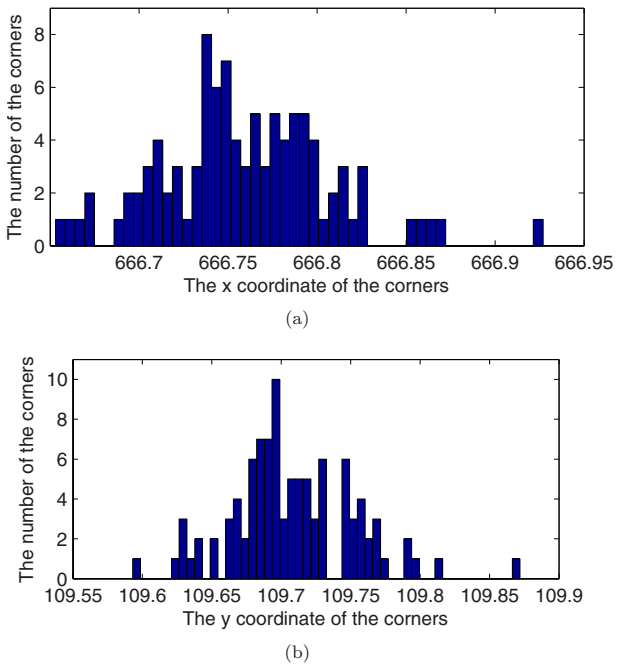

Fig. 13 Histograms of the frequency counts for one corner point for (a) the *x* coordinate and (b) the *y* coordinate.

noise; nevertheless, the reprojection error on the projector image is the result of coupling both the SLS system parameters and the measurement noise. Because of coupling effect, the statistical characteristics of the reprojection error is not determined. Thus, calibrating the projector from the camera image point of view is direct and easy to be understood in the sense of the statistics. Second, more data can increase the precision. Not only the projector feature points but also the 3-D plane points are applied to estimate the parameters in our method.

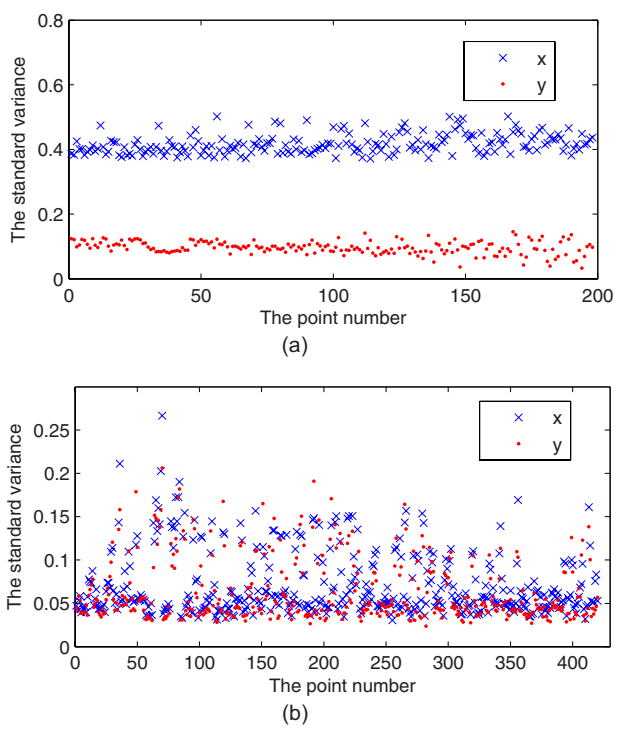

Fig. 14 Noise of the corners for (a) the camera calibration image and (b) the projector calibration image.

If we do not know the statistical characteristics of the measurement noise, the idea of the calibration from the camera image using the nonlinear least-squares method is also valuable. If the real noise statistical characteristics is known, the proposed idea also has a great advantage, because we can not know the statistical characteristics of the reprojection error on the projector image. We believe that a higher precision estimation will be obtained from the camera image than that from the projector image using the bundle adjustment.

6 Conclusions

We proposed a method to estimate the projector parameters according to the camera image reprojection error. It does not require us to know the statistical characteristics of the projector image point and makes full use of the background knowledge of the camera image noise. The simulations and real experiments affirmed that estimation of the projector on the camera image has a higher precision.

Although we used the planar target and the nonlinear projector model in this paper, the idea, calibrating from the camera image point of view, is also suitable for 3-D reference objects and other projector models. For the 3-D reference objects, it just required us to modify the transformation function. For the line model and plane model, the least-squares method in the 3-D space could be applied to acquire the initial parameter values; while for the pinhole model, the least-squares method the in 2-D space of the projector image achieved good initial values. Then the bundle adjustment on the camera image could be applied to improve the precision of the estimates.

Acknowledgments

This work was partially supported by the National Key Basic Research Program under Grant No. 2007CB714005, the National Natural Science Foundation of China under Grant Nos. 50821003 and 50775147, and the Science & Technology Commission of Shanghai Municipality under Grant No. 07JC14028.

References

1. F. Chen, G. M. Brown, and M. Song, "Overview of three-dimensional shape measurement using optical method," *Opt. Eng.* **39**(1), 10–22 (2000).
2. M. Ribo and M. Brandner, "State of the art on vision-based structured light systems for 3D measurements," in *Proc. 2005 IEEE Int. Workshop on Robotic Sensors: Robotic and Sensor Environments*, pp. 2–7 (2005).
3. F. Blais, "Review of 20 years of range sensor development," *J. Electron. Imaging* **13**(1), 231–243 (2004).
4. N. D'Apuzzo, "Overview of 3D surface digitization technologies in Europe," *Proc. SPIE* **6056**, 605605 (2006).
5. T. Clarke and J. Fryer, "The development of camera calibration methods and models," *Photogramm. Rec.* **16**(91), 51–66 (1998).
6. J. Salvi, X. Armangue, and J. Batlle, "A comparative review of camera calibrating methods with accuracy evaluation," *Pattern Recogn.* **35**(7), 1617–1635 (2002).
7. R. Tsai, "A versatile camera calibration technique for high-accuracy 3D machine vision metrology using off-the-shelf TV cameras and lenses," *IEEE J. Rob. Autom.* **3**(4), 323–344 (1987).
8. Z. Zhang, "A flexible new technique for camera calibration," *IEEE Trans. Pattern Anal. Mach. Intell.* **22**(11), 1330–1334 (2000).

9. S. Joaquim, P. Jordi, and B. Joan, "Pattern codification strategies in structured light systems," *Pattern Recogn.* **37**(4), 827–849 (2004).
10. R. Dewar, "Self-generated targets for spatial calibration of structured light optical sectioning sensors with respect to an external coordinate system," in *Proc. Robots and Vision '88 Conf.*, pp. 5–13, Society of Manufacturing Engineers (1988).
11. K. James, "Noncontact machine vision metrology within a CAD coordinate system," in *Proc. Autofact'88 Conf.*, Vol. **12**, pp. 9–17, Society of Manufacturing Engineers, Computer and Automated Systems Association of SME (1988).
12. F. Marzani, Y. Voisin, L. Voon, and A. Diou, "Calibration of a three-dimensional reconstruction system using a structured light source," *Opt. Eng.* **41**, 484–492 (2002).
13. I. Reid, "Projective calibration of a laser-stripe range finder," *Image Vis. Comput.* **14**(9), 659–666 (1996).
14. C. Chen and A. Kak, "Modeling and calibration of a structured light scanner for 3-D robot vision," in *Proc. 1987 IEEE Int. Conf. on Robotics and Automation*, Vol. **4**, pp. 807–815 (1987).
15. D. Huynh, R. Owens, and P. Hartmann, "Calibrating a structured light stripe system: a novel approach," *Int. J. Comput. Vis.* **33**(1), 73–86 (1999).
16. F. Zhou and G. Zhang, "Complete calibration of a structured light stripe vision sensor through planar target of unknown orientations," *Image Vis. Comput.* **23**(1), 59–67 (2005).
17. R. Legarda-Sáenz, T. Bothe, and W. Jüptner, "Accurate procedure for the calibration of a structured light system," *Opt. Eng.* **43**(2), 464–471 (2004).
18. Z. Song and R. Chung, "Use of LCD panel for calibrating structured-light-based range sensing system," *IEEE Trans. Instrum. Meas.* **57**(11), 2623–2630 (2008).
19. S. Zhang and P. Huang, "Novel method for structured light system calibration," *Opt. Eng.* **45**(8), 083601 (2006).
20. K. Yamauchi, H. Saito, and Y. Sato, "Calibration of a structured light system by observing planar object from unknown viewpoints," in *Proc. 19th Int. Conf. on Pattern Recognition*, pp. 1–4, IEEE Computer Society (2008).
21. W. Schreiber and G. Notni, "Theory and arrangements of self-calibrating whole-body three-dimensional measurement systems using fringe projection technique," *Opt. Eng.* **39**(1), 159–169 (2000).
22. D. Fofi, J. Salvi, and E. Mouaddib, "Uncalibrated reconstruction: an adaptation to structured light vision," *Pattern Recogn.* **36**(7), 1631–1644 (2003).
23. R. Furukawa and H. Kawasaki, "Uncalibrated multiple image stereo system with arbitrarily movable camera and projector for wide range scanning," in *Proc. 5th Int. Conf. on 3-D Digital Imaging and Modeling*, pp. 302–309 (2005).
24. B. Triggs, P. McLauchlan, R. Hartley, and A. Fitzgibbon, "Bundle adjustment-a modern synthesis," *Lect. Notes Comput. Sci.* **1883**, 298–372 (1999).
25. J. Heikkila, "Geometric camera calibration using circular control points," *IEEE Trans. Pattern Anal. Mach. Intell.* **22**(10), 1066–1077 (2000).
26. D. Gennery, "Least-squares camera calibration including lens distortion and automatic editing of calibration points," in *Calibration and Orientation of Cameras in Computer Vision*, A. Gruen and T. S. Huang, Eds., pp. 123–136, Springer-Verlag, Berlin, Hiedelberg (2001).
27. J. J. Mor, "The Levenberg-Marquardt algorithm: implementation and theory," *Lect. Notes Math.* **630**, 105–116 (1977).
28. C. Slama, C. Theurer, and S. Henriksen, *Manual of Photogrammetry*, American Society of Photogrammetry, Falls Church, VA (1980).
29. L. M. Zhu, H. G. Luo, and X. Zhang, "Uncertainty and sensitivity analysis for camera calibration," *Indust. Robot Int. J.* **36**(3), 238–243 (2009).
30. F. MacWilliams and N. Sloane, "Pseudo-random sequences and arrays," *Proc. IEEE* **64**(12), 1715–1729 (1976).
31. R. Deriche and G. Giraudon, "Accurate corner detection: an analytical study," in *Proc. 3rd Int. Conf. on Computer Vision*, pp. 66–70, IEEE Computer Society (1990).

Xu Zhang is a PhD student in the Robotics Institute, Shanghai Jiao Tong University, China. His interests include range sensing and computer vision.

Limin Zhu received his BE (with honors) and PhD degrees in mechanical engineering from the Southeast University, Nanjing, China, in 1994 and 1999, respectively. From November 1999 to January 2002, he was a postdoctoral research fellow with Huazhong University of Science and Technology, Wuhan, China. In March 2002, he became an associate professor with the Robotics Institute, School of Mechanical Engineering, Shanghai Jiao Tong University, China, where he has been a professor since August 2005. He held a visitorship with Monash University, Clayton, Australia, from September 1997 to May 1998 and with The City University of Hong Kong, Kowloon, from December 2000 to March 2001. His research interests include robotic vision, numerical control (NC) programming, and mechanical signature analysis.